The Canadian Mineralogist
Vol. 54, pp. 827-845 (2016)
DOI: 10.3749/canmin.1600016

TRIPHYLITE–SARCOPSIDE MISCIBILITY GAP IN THE FeO–MnO–Li_2O–P_2O_5–H_2O SYSTEM: EXPERIMENTAL INVESTIGATION AND THERMOMETRIC APPLICATION TO GRANITIC PEGMATITES

FREDERIC HATERT[§]

Laboratoire de Minéralogie, Département de Géologie, Bâtiment B18, Université de Liège, B-4000 Liège, Belgium

ENCARNACIÓN RODA-ROBLES

Departamento de Mineralogía y Petrología, Univ. País Vasco (UPV/EHU), P.O. Box 644, E-48080 Bilbao, Spain

LUISA OTTOLINI

C.N.R.-Istituto di Geoscienze e Georisorse (IGG), Unità di Pavia, Via A. Ferrata 1, I-27100 Pavia, Italy

PETER SCHMID-BEURMANN

Institute für Mineralogie, Correnssstrasse 24, 48149 Münster, Germany

MAXIME BAIJOT AND FABRICE DAL BO

Laboratoire de Minéralogie, Département de Géologie, Bâtiment B18, Université de Liège, B-4000 Liège, Belgium

ABSTRACT

In order to assess the stability of the primary triphylite + sarcopside assemblage, we performed hydrothermal experiments between 400 and 700 °C (Ni/NiO oxygen fugacity buffer, $P = 1$ kbar), starting from the $Li(Fe^{2+}_{2.5-x}Mn^{2+}_{x})(PO_4)_2$ ($x = 0.0$, 0.5, 1.0) compositions, which represent the ideal compositions of triphylite + sarcopside assemblages in which both minerals occur in a 1:1 molar ratio. The triphylite + sarcopside assemblage is observed in all experiments, associated with other phosphates like $(Fe^{2+},Mn^{2+})_2P_2O_7$, $(Fe^{2+},Mn^{2+})Fe^{3+}_2(PO_4)_2(OH)_2{\cdot}nH_2O$, or $Fe^{3+}_4(Fe^{2+},Mn^{2+})_3(PO_4)_6$. Electron-microprobe and SIMS analyses show a progressive decrease of the Li contents in the triphylites, balanced by an increase of their Fe^{2+}-contents, when the temperature increases. These compositional changes are due to the increase of the triphylite–sarcopside miscibility along the $Li_2(Fe^{2+},Mn^{2+})_2(PO_4)_2$–$Fe^{2+}(Fe^{2+},Mn^{2+})_2(PO_4)_2$ solid solution; the experimental phase diagrams can consequently be used as a geothermometer to calculate the exsolution temperatures of the assemblages. A linear fit of the experimental data leads to the general equation: T (°C) = (–142 * XFe) – (773 * Li *pfu*) + 1131, where XFe = Fe/(Fe + Mn). The uncertainty is around ±15 °C, and the influence of pressure is assumed to be negligible. By using this equation, exsolution temperatures were calculated for nine triphylite–sarcopside assemblages from pegmatites; these temperatures do not represent the crystallization temperatures of the phosphate nodules, but correspond to the closing temperature of the triphylite–sarcopside element exchange. Nevertheless, these temperatures, between 276 and 397 °C, are in fairly good agreement with those generally accepted for the crystallization of primary phosphate assemblages in granitic pegmatites.

Keywords: triphylite, sarcopside, Li-Mn-Fe^{2+} phosphates, granitic pegmatites, phase relations, geothermometry, SIMS.

[§] *Corresponding author e-mail address*: fhatert@ulg.ac.be

Introduction

In rare-element pegmatites of the beryl-columbite-phosphate and spodumene subtypes (Černý & Ercit 2005) members of the triphylite–lithiophilite series [$LiFe^{2+}(PO_4)$–$LiMn^{2+}(PO_4)$] are the most common primary (magmatic) Fe-Mn phosphate minerals. They occur as masses enclosed in silicates that can attain several meters in diameter, and petrographic investigations of the phosphate minerals are used by mineralogists as a tool to decipher the transformation sequences affecting pegmatites during their evolution.

Petrographic observations of the Fe-Mn phosphates have revealed lamellar textures involving minerals of the triphylite–lithiophilite and sarcopside–zavalíaite [$Fe^{2+}{}_3(PO_4)_2$–$Mn^{2+}{}_3(PO_4)_2$] series (Fransolet 1977, Smeds *et al*. 1998, Roda-Robles *et al*. 2010 and 2011, Hatert *et al*. 2012b). According to Moore (1972), all petrographic evidence shows that the sarcopside lamellae are an exsolution product, thus indicating that an extensive solid solution between triphylite and sarcopside certainly exists at high temperature. In triphylite/graftonite [$(Fe^{2+},Mn^{2+},Ca)_3(PO_4)_2$] exsolution textures, tiny sarcopside lamellae frequently appear in triphylite lamellae (Roda-Robles *et al*. 2010); they were produced by an exsolution process similar to that described herein.

Since the petrogenetic significance of accessory phosphate minerals in pegmatites has been demonstrated in the ultrahigh-pressure rocks of the Dora-Maira massif, Italy (Brunet *et al*. 1998), it now clearly appears that experimental studies of these rare minerals are necessary to better understand the genesis of pegmatites (London *et al*. 1999, 2001). With this goal in mind, Hatert *et al*. (2006) investigated experimentally the $Na_2(Mn^{2+}{}_{1-x}Fe^{2+}{}_x)_2Fe^{3+}(PO_4)_3$ series ($x = 0$ to 1), which models the chemical compositions of natural, weakly oxidized, primary alluaudites. More recently, the hydrothermal experiments performed by Hatert *et al*. (2011, 2014) in the $LiNa_2Mn^{2+}{}_xFe^{2+}{}_{3-x}Fe^{3+}(PO_4)_4$ ($x = 1.054$, 1.502, 1.745) and Na–Fe^{2+}–Fe^{3+}(+PO_4) systems allowed us to develop a new geothermometer based on the Na content of triphylite, and to shed some light on the stability of Fe-rich alluaudites.

In order to corroborate the existence of primary triphylite + sarcopside assemblages in pegmatites, and to determine the extent of the triphylite–sarcopside solid solution, we decided to perform hydrothermal experiments between 400 and 700 °C at 1 kbar, in the $Li_2(Fe^{2+},Mn^{2+})_2(PO_4)_2$–$Fe^{2+}(Fe^{2+},Mn^{2+})_2(PO_4)_2$ system. The aim of this paper is to illustrate the results of these experiments, which will provide a tool for constraining the temperature that prevailed in pegmatites during the crystallization of the triphylite + sarcopside assemblage.

Experimental Procedure

The hydrothermal experiments were performed between 400 and 700 °C at 1 kbar, starting from $Li(Fe^{2+}{}_{2.5-x}Mn^{2+}{}_x)(PO_4)_2$ ($x = 0.0$, 0.5, 1.0), which represents the ideal compositions of triphylite + sarcopside assemblages in which both minerals occur in a 1:1 molar ratio. Manganese was introduced to the system to better model compositions of natural assemblages. Stoichiometric quantities of Li_3PO_4, $FePO_4$, $Mn_3(PO_4)_2$, and metallic Fe (Merck, Darmstadt, Germany, min. 99.5%) were homogenized in a mortar in acetone. Li_3PO_4, $Fe^{3+}PO_4$, and $Mn^{2+}{}_3(PO_4)_2$ were previously synthesized by solid-state reaction in air, starting from stoichiometric mixtures of $NH_4H_2PO_4$ (Merck, min. 99%), Li_2CO_3 (Merck, Darmstadt, Germany, 99.99%), Fe_2O_3 (Acros, Geel, Belgium, 99.999%), and MnO (Alfa, Karsruhe, Germany, 99.5%), which were heated in a platinum crucible for 1 to 2 days. The final synthesis temperatures were 800 °C (Li_3PO_4), 950 °C ($Fe^{3+}PO_4$), and 900 °C [$Mn^{2+}{}_3(PO_4)_2$], and the purity of the synthesized phosphates was confirmed by X-ray powder diffraction.

Approximately 20 to 30 mg of the starting materials were welded, together with 2 μL of distilled water, into small gold tubes with an outer diameter of 2 mm, a wall thickness of 0.1 mm, and a length of 25 mm. The capsules were then inserted into a conventional hydrothermal apparatus with vertically arranged Tuttle-type cold-seal bombs (Tuttle 1949) for seven days, and then cooled in a stream of cold air. The pressure media was water, and the oxygen fugacity was buffered by the bomb to a value close to that of the Ni-NiO buffer (O'Neill & Pownceby 1993). Pressure and temperature errors are estimated to be within ±3% and ±10 °C, respectively.

Analytical Procedures

The X-ray powder diffraction patterns of the synthesized compounds were recorded with a Philips PW-3710 diffractometer located in Liège, Belgium, using 1.9373 Å Fe$K\alpha$ radiation. The unit-cell parameters were calculated with the LCLSQ 8.4 least-squares refinement program (Burnham 1991) from the *d*-spacings calibrated with $Pb(NO_3)_2$ as an internal standard. Structure refinements were performed by the Rietveld technique (Rietveld 1967, 1969) with the DBWS program (Young *et al*. 1998).

Electron-microprobe analyses of natural and synthetic phosphates were performed with Cameca SX-50 instruments located in Bochum, Germany (analyst H.-J.

TABLE 1. RESULTS OF SYNTHESIS EXPERIMENTS USING THE $Li(Fe^{2+}_{2.5-x}Mn^{2+}_{x})(PO_4)_2$ STARTING COMPOSITIONS ($x = 0.0, 0.5, 1.0$)

Starting compositions	T (°C)	P (kbar)	Duration (days)	Products	Exp. no.
$LiFe^{2+}_{2.5}(PO_4)_2$	400	1	7	Triphylite + sarcopside + $Fe^{3+}_4Fe^{2+}_3(PO_4)_6$ + $Fe^{2+}Fe^{3+}_2(PO_4)_2(OH)_2 \bullet nH_2O$	H.302
($x = 0.0$)	500	1	7	Triphylite + sarcopside + $Fe^{2+}_2P_2O_7$	H.297
	600	1	7	Triphylite + sarcopside + $Fe^{2+}Fe^{3+}_2(PO_4)_2(OH)_2 \bullet nH_2O$	H.303
	700	1	7	Triphylite + sarcopside + $Fe^{2+}_2P_2O_7$ (tr.)	H.298
$LiFe^{2+}_2Mn^{2+}_{0.5}(PO_4)_2$	400	1	7	Triphylite + sarcopside + $(Fe^{2+},Mn^{2+})Fe^{3+}_2(PO_4)_2(OH)_2 \bullet nH_2O$ + $Fe^{3+}_4(Fe^{2+},Mn^{2+})_3(PO_4)_6$ (tr.)	H.304
($x = 0.5$)	500	1	7	Triphylite + sarcopside	H.312
	600	1	7	Triphylite + sarcopside + $(Fe^{2+},Mn^{2+})Fe^{3+}_2(PO_4)_2(OH)_2 \bullet nH_2O$ (tr.)	H.305
	700	1	7	Triphylite + sarcopside + $(Fe^{2+},Mn^{2+})Fe^{3+}_2(PO_4)_2(OH)_2 \bullet nH_2O$	H.311
$LiFe^{2+}_{1.5}Mn^{2+}(PO_4)_2$	400	1	7	Triphylite + sarcopside + $(Fe^{2+},Mn^{2+})Fe^{3+}_2(PO_4)_2(OH)_2 \bullet nH_2O$ + $(Fe^{2+},Mn^{2+})_2P_2O_7$	H.306
($x = 1.0$)	500	1	7	Triphylite + sarcopside + $(Fe^{2+},Mn^{2+})_2P_2O_7$ + $(Fe^{2+},Mn^{2+})Fe^{3+}_2(PO_4)_2(OH)_2 \bullet nH_2O$ (tr.)	H.314
	600	1	7	Triphylite + sarcopside + $Fe^{3+}_4(Fe^{2+},Mn^{2+})_3(PO_4)_6$ + $(Fe^{2+},Mn^{2+})Fe^{3+}_2(PO_4)_2(OH)_2 \bullet nH_2O$ (tr.)	H.307
	700	1	1	Triphylite + sarcopside + $Fe^{3+}_4(Fe^{2+},Mn^{2+})_3(PO_4)_6$ + $(Fe^{2+},Mn^{2+})Fe^{3+}_2(PO_4)_2(OH)_2 \bullet nH_2O$	H.313

Bernhardt), and in Toulouse, France (analyst P. de Parseval), which operated in the wavelength-dispersion mode with an accelerating voltage of 15 kV, a beam current of 15 nA, and a beam diameter of 5 μm. The standards used were graftonite from Kabira (sample KF16, Fransolet 1975) (for Fe, Mn, P), pyrope (Mg), ZnO (Zn), and andradite (Ca).

The Li_2O contents were determined with a Cameca IMS 4f ion microprobe (SIMS) at the Consiglio Nazionale delle Ricerche-Instituto di Geoscienze e Georisorse (CNR-IGG), Pavia, Italy. We used a 12.5 kV-accelerated $^{16}O^-$ primary ion beam with a current intensity in the range 0.8–4 nA, corresponding to a beam diameter of 3–6 μm. The samples were polished, washed in an ultrasonic bath with ethanol, and Pt-coated (400 Å thickness) before analysis. Secondary-ion signals of the $^6Li^+$, $^{31}P^+$, and $^{57}Fe^+$ isotopes were detected at the electron multiplier. Acquisition times were 3 s for Li and P (each), and 6 s for Fe over three cycles. Analyses were done under steady state sputtering conditions after 360 s sputtering using ~75–125 eV secondary ions. The choice of medium-to-high-energy (energy filtering) secondary ions as analytical ones is particularly useful to reduce the matrix effects affecting light-element ionization and improve the reproducibility of analysis (Ottolini *et al*. 1993). We used triphylite from the Buranga pegmatite, Rwanda, as reference material for SIMS Li-analyses; more details concerning the SIMS analytical procedure are given by Hatert *et al*. (2011, 2012a). For Li_2O concentration values at the percent level, the analytical uncertainty is always very low, *i.e*., few percent relative or lower, as 1 standard deviation %.

Modal proportions of triphylite (or ferrisicklerite) and sarcopside were determined from the thin sections with a polarizing microscope, using classical point-counting methods.

Phase Characterization

Triphylite-type phosphates

Triphylite-type phosphates were observed in all hydrothermal experiments performed in this study, from 400 to 700 °C (Table 1). At low temperatures of 400 and 500 °C, the triphylite grains show an average diameter of *ca*. 20–30 μm, and are finely intergrown with sarcopside and $(Fe^{2+},Mn^{2+})Fe^{3+}_2(PO_4)_2(OH)_2 \bullet nH_2O$ (Fig. 1a), whereas at 600 and 700 °C the triphylite occurs as round crystals up to 50 μm in diameter (Fig. 1b). In these high-temperature experiments, crystal aggregates were also observed, which are composed of an intricate assemblage of irregular triphylite and sarcopside grains (Fig. 1c). In an experiment performed at 700 °C, starting from the composition $LiFe^{2+}_{2.5}(PO_4)_2$ (H.298), triphylite and sarcopside form round grains, which are not distinguishable in backscattered electron images, or by electron-microprobe analysis (Fig. 1d; Table 2).

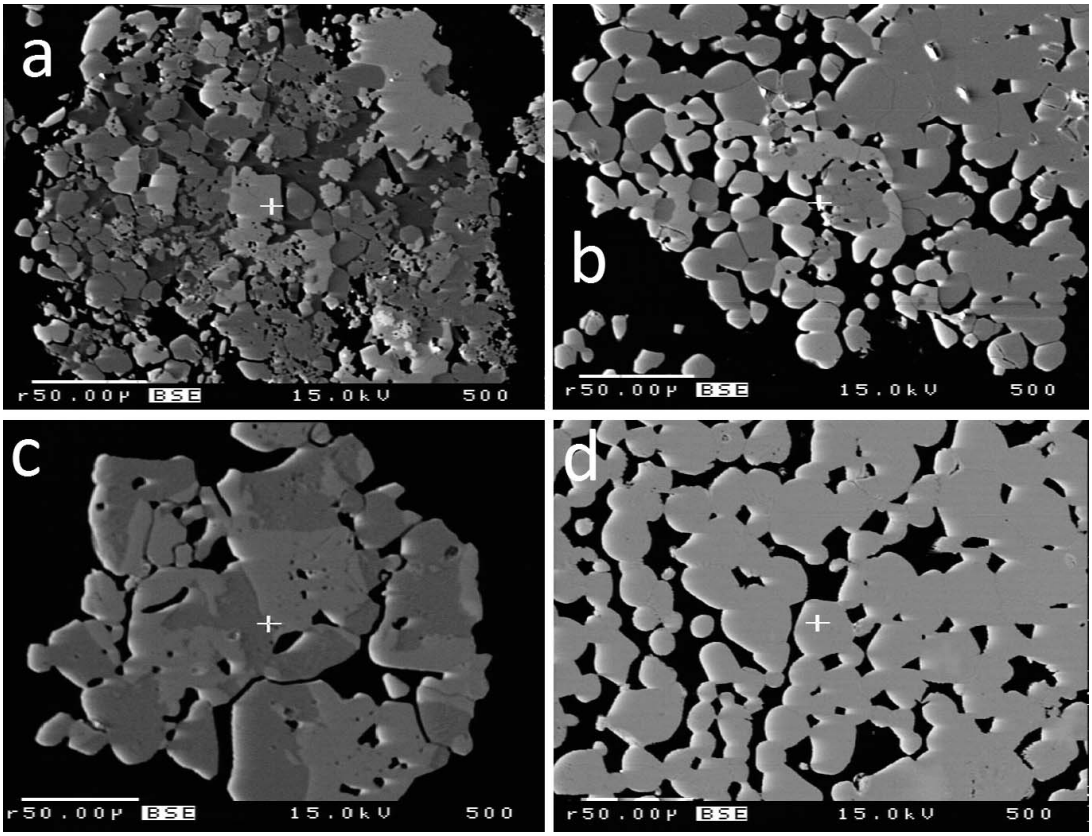

FIG. 1. (a) Assemblage of irregular and small triphylite (medium gray) and $Fe^{2+}Fe^{3+}{}_2(PO_4)_2(OH)_2 \bullet nH_2O$ grains (dark gray), associated with larger sarcopside grains (light gray), obtained at 400 °C from the $LiFe^{2+}{}_{2.5}(PO_4)_2$ composition. Sample H.302, scanning electron microscope, backscattered electron image. (b) Round grains of triphylite (dark gray) and sarcopside (light gray), obtained at 700 °C from the $LiFe^{2+}{}_{1.5}Mn^{2+}(PO_4)_2$ composition. Sample H.313, scanning electron microscope, backscattered electron image. (c) Intricate assemblage of large triphylite (dark gray) and sarcopside (light gray) crystals, obtained at 600 °C from the $LiFe^{2+}{}_{2.5}(PO_4)_2$ composition. Sample H.303, scanning electron microscope, backscattered electron image. (d) Round grains of triphylite and sarcopside, which exhibit the same chemical composition and are not distinguishable in the backscattered electron images. These grains were synthesized at 700 °C from the $LiFe^{2+}{}_{2.5}(PO_4)_2$ composition. Sample H.298, scanning electron microscope, backscattered electron image.

However, the presence of both phases was confirmed by X-ray powder diffraction data.

Electron-microprobe and SIMS analyses of the experimental products show Fe/(Fe + Mn) ratios from 0.554 to 1.000, as well as Li contents evolving from 6.76–8.56 wt.% Li_2O at 400 °C to 3.32–5.55 wt.% Li_2O at 700 °C (Table 2). As shown in Figure 2, this decreasing Li content in triphylite is correlated with an increase of the (Fe + Mn) content, according to the substitution mechanism $Li^+ + Li^+ \rightarrow (Fe,Mn)^{2+} + \square$. Starting from the ideal formula of triphylite, $LiFe^{2+}(PO_4)$, this substitution mechanism explains compositional variations evolving towards sarcopside, which can be expressed as $\square_{0.5}Fe^{2+}{}_{1.5}(PO_4)$. A general formula for the solid solutions with respect to the endmembers $LiFe^{2+}(PO_4)$ and $\square_{0.5}Fe^{2+}{}_{1.5}(PO_4)$ can therefore be formulated as $\square_{0.5-z/2}Li_zFe^{2+}{}_{1.5-z/2}(PO_4)$, where z equals the molar ratio of the $LiFe^{2+}(PO_4)$ component.

Unit-cell parameters of the synthesized triphylite-type phosphates are given in Table 3, and the unit-cell volume shows a rather good correlation with the Fe/(Fe + Mn) ratio (Fig. 3). The scatter of the data points is due to variable Li contents, but the absence of satisfactory correlation between the unit-cell volume and these Li contents indicates that unit-cell parameters of triphylite-type phosphates are more strongly

TABLE 2. CHEMICAL COMPOSITIONS OF TRIPHYLITE-TYPE PHOSPHATES, HYDROTHERMALLY SYNTHESIZED FROM THE $Li(Fe^{2+}_{2.5-x}Mn^{2+}_{x})(PO_4)_2$ STARTING COMPOSITIONS ($x = 0.0, 0.5, 1.0$)

Exp. no.	H.302	H.297	H.303	H.298	H.304	H.312	H.305	H.311	H.306	H.314	H.307	H.313
No. of analyses	17	15	17	27	19	17	19	17	12	14	23	24
x	0.0	0.0	0.0	0.0	0.5	0.5	0.5	0.5	1.0	1.0	1.0	1.0
T (°C)	400	500	600	700	400	500	600	700	400	500	600	700
P_2O_5 (wt.%)	43.06	43.63	42.05	42.71	45.31	43.10	43.21	41.39	44.48	44.78	43.86	41.87
FeO	48.07	50.32	52.18	53.48	37.77	40.34	41.79	42.10	25.96	28.84	32.73	32.58
MnO	0.00	0.00	0.00	0.00	9.07	9.24	10.28	10.92	20.63	19.74	17.79	18.14
Li_2O[a]	6.76	6.01	4.31	3.32	7.19	6.25	4.58	3.94	8.56	6.15	5.71	5.55
	± 0.39	± 0.31	± 0.43	± 0.15		± 0.26	± 0.14	± 0.34		± 0.30	± 0.14	± 0.22
Total	97.89	99.96	98.54	99.51	99.34	98.93	99.86	98.35	99.63	99.51	100.09	98.14
Cation numbers calculated on the basis of 4 O per formula unit												
P (*apfu*)	1.006	1.008	1.008	1.020	1.025	1.004	1.014	1.001	1.001	1.025	1.012	0.996
Fe^{2+}	1.110	1.149	1.235	1.262	0.844	0.928	0.969	1.006	0.577	0.652	0.746	0.765
Mn^{2+}	0.000	0.000	0.000	0.000	0.205	0.215	0.241	0.264	0.464	0.452	0.411	0.432
Li	0.750	0.660	0.491	0.376	0.773	0.692	0.510	0.453	0.915	0.669	0.626	0.627
Fe/(Fe + Mn)	1.000	1.000	1.000	1.000	0.804	0.812	0.801	0.792	0.554	0.590	0.645	0.639

Analysts H.-J. Bernhardt (Bochum, Germany) and P. de Parseval (Toulouse, France).

[a] The Li_2O content was determined by SIMS (Analyst L. Ottolini, Pavia, Italy) and the error represents (1σ) standard deviation.

TABLE 3. UNIT-CELL PARAMETERS OF THE PHOSPHATES HYDROTHERMALLY SYNTHESIZED FROM THE $Li(Fe^{2+}_{2.5-x}Mn^{2+}_{x})(PO_4)_2$ STARTING COMPOSITIONS (x = 0.0, 0.5, 1.0)

Exp. no.	*a* (Å)	*b* (Å)	*c* (Å)	β (°)	*V* (Å^3)
Triphylites					
H.297	4.706(2)	10.35(1)	6.010(3)	90.00	292.8(6)
H.298	4.701(2)	10.37(1)	6.011(4)	90.00	293.0(7)
H.302	4.702(3)	10.33(1)	6.007(5)	90.00	291.9(9)
H.303	4.696(2)	10.36(1)	6.009(4)	90.00	292.3(6)
H.304	4.712(4)	10.36(2)	6.001(6)	90.00	292.8(9)
H.305	4.710(4)	10.42(2)	5.977(7)	90.00	293(1)
H.306	4.726(3)	10.41(1)	5.969(4)	90.00	293.6(8)
H.307	4.727(5)	10.42(2)	5.973(8)	90.00	294(1)
H.311	4.712(3)	10.42(1)	5.973(5)	90.00	293.2(8)
H.312	4.708(4)	10.41(2)	5.978(6)	90.00	293(1)
H.313	4.730(3)	10.42(1)	5.981(5)	90.00	294.7(8)
H.314	4.732(3)	10.42(1)	5.982(5)	90.00	294.8(8)
Sarcopsides					
H.297	6.058(6)	4.776(4)	10.41(2)	90.5(1)	301.2(4)
H.298	6.060(4)	4.771(3)	10.40(1)	90.5(1)	300.6(3)
H.302	6.069(7)	4.772(6)	10.45(1)	90.6(1)	302.6(5)
H.303	6.035(7)	4.778(4)	10.37(2)	90.6(2)	299.0(4)
H.304	6.091(5)	4.796(3)	10.448(8)	90.4(1)	305.2(3)
H.305	6.083(3)	4.786(2)	10.45(1)	90.37(8)	304.3(3)
H.306	6.096(2)	4.808(1)	10.514(3)	89.25(3)	308.1(1)
H.307	6.07(2)	4.72(2)	10.75(3)	87.8(4)	308(1)
H.311	6.077(5)	4.792(4)	10.44(2)	90.4(1)	304.1(5)
H.312	6.080(5)	4.791(3)	10.46(2)	90.4(1)	304.7(5)
H.313	6.10(3)	4.74(2)	10.73(4)	87.8(5)	310(1)
H.314	6.091(4)	4.807(3)	10.501(8)	89.04(5)	307.4(2)

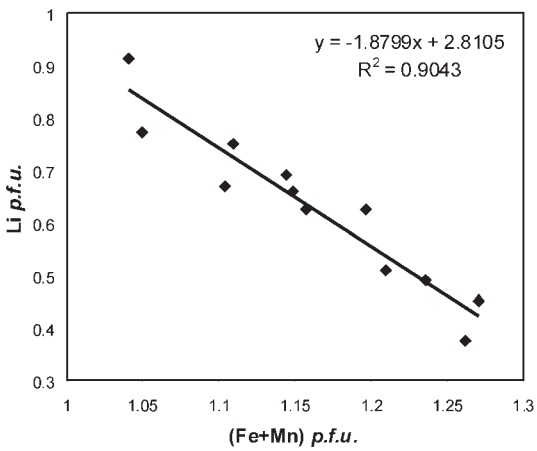

FIG. 2. Correlation between the Li and (Fe + Mn) contents in synthetic triphylites (atoms per formula unit, *apfu*).

influenced by their Fe/(Fe + Mn) ratio than by their Li content.

Sarcopside-type phosphates

The hydrothermal experiments performed in the present study showed the presence of sarcopside-type phosphates associated with triphylite at all temperatures (Table 1). Sarcopside forms colorless grains reaching 50 μm, showing an irregular shape at 400 and 500 °C (Fig. 1a), and a more euhedral and round equant shape at 600 and 700 °C (Fig. 1b, d). The electron-microprobe analyses (Table 4) show Fe/(Fe + Mn) ratios between 0.508 and 1.000, which is in fairly good agreement with the Fe/(Fe + Mn) ratios calculated from the unit-cell parameters (Table 3) using the empirical correlations established by Rondeux (2011). The Li_2O contents of the sarcopside range from 0.09 to 0.80 wt.%, and no correlation was observed between this Li concentration and the temperature (Table 4). The incorporation of lithium into the sarcopside structure, reported here for the first time, is achieved by the replacement of Fe^{2+},

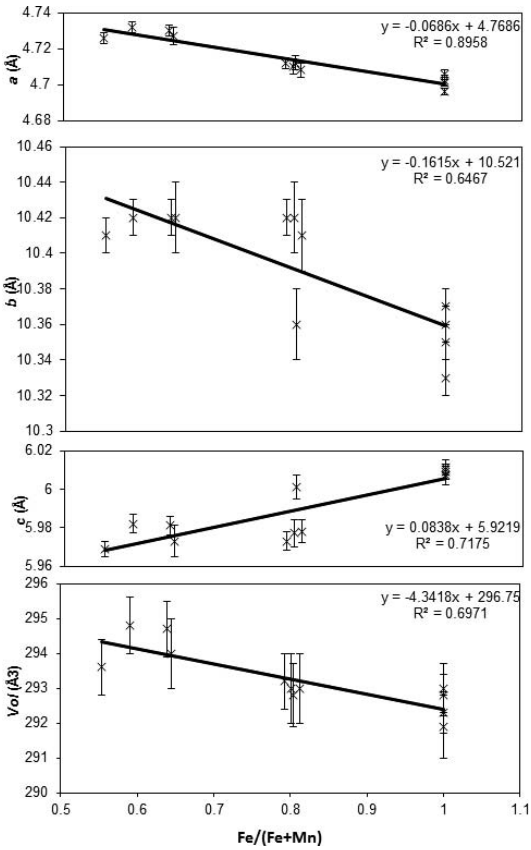

FIG. 3. Variation between the unit-cell parameters of synthetic triphylites and their Fe/(Fe + Mn) contents.

according to the substitution mechanism $Fe^{2+} + \square \rightarrow Li^{+} + Li^{+}$.

$(Fe^{2+},Mn^{2+})Fe^{3+}{}_2(PO_4)_2(OH)_2 \cdot nH_2O$

A dark phosphate, forming euhedral crystals attaining 100 μm in length (Figs. 1a, 4a), was observed in several experiments performed from 400 to 700 °C (Table 1). This phase appears dark gray in backscattered electron mode microscopy, indicating that it contains a significant amount of a low mean-atomic mass component. This inference is confirmed by the low totals of the electron-microprobe analyses, ranging from 82.27 to 85.47 wt.% (Table 5). Moreover, qualitative SIMS analyses of H in this matrix allowed us to detect H^{+} current intensity higher by orders of magnitude than that monitored in the other Li-bearing phases investigated here. The lack of Li-phosphates with well-characterized water content, to be used for H calibration, prevented us from obtaining quantitative determination of H_2O concentration in this phosphate.

A few lines observed on the X-ray powder diffraction patterns of the experimental products allowed us to identify this phase as a laueite-type phosphate. The composition, calculated from the chemical data on the basis of 2 P atoms *pfu*, is $(Fe^{2+},Mn^{2+})_{0.72–1.25}Fe^{3+}{}_{1.83–2.19}(PO_4)_2(OH)_2 \bullet 2.47–3.52H_2O$, with a $Fe_{total}/(Fe_{total} + Mn)$ ratio between 0.771 and 1.000 (Table 5). This formula is in fairly good agreement with the ideal formula of laueite-type phosphates, $(Fe^{2+},Mn^{2+})Fe^{3+}{}_2(PO_4)_2(OH)_2 \bullet 8H_2O$, even if the H_2O contents, calculated by difference to 100 wt.%, are significantly lower in the synthetic phosphates. This feature can be explained by water loss during the electron-microprobe analyses, since the phosphate was strongly damaged under the electron beam. Moreover, the number of water molecules in natural laueite is also lower than the ideal values, with contents around 6.2 H_2O molecules *pfu* (Moore 1965).

$Fe^{3+}{}_4(Fe^{2+},Mn^{2+})_3(PO_4)_6$

Several experiments performed between 400 and 700 °C show the presence of large euhedral black crystals attaining 200 μm in length with compositions of $Fe^{3+}{}_4(Fe^{2+},Mn^{2+})_3(PO_4)_6$ (Table 1). Identification of this phosphate was confirmed by X-ray powder diffraction, and the electron-microprobe analyses (Table 5) indicate compositions in which (Fe + Mn) is between 7.02 and 7.30 *apfu*, with the Fe/(Fe + Mn) ratios ranging from 0.629 to 1.000. It is noteworthy that significant amounts of Li have been observed in this phase, attaining 0.776 Li atoms *pfu* (Table 5). Phosphates characterized by the same structure type are frequently reported in the literature (Belfguira *et al*. 2010, Dal Bo & Hatert 2012).

$(Fe^{2+},Mn^{2+})_2P_2O_7$

$(Fe^{2+},Mn^{2+})_2P_2O_7$ was observed in several experiments between 400 and 700 °C (Table 1) as colorless euhedral crystals attaining 50 μm in size (Fig. 4b). They were identified by X-ray powder diffraction, and the electron-microprobe analyses (Table 5) indicate Fe/(Fe + Mn) ratios from 0.127 to 1.000. Similar crystals were previously synthesized by Stefanidis & Nord (1982, 1984) and Hatert *et al*. (2006).

Natural triphylite + sarcopside assemblages

Minerals of the triphylite-lithiophilite and sarcopside-zavalíaite series are commonly associated in pegmatites, where they generally form the exsolution textures extensively described in the literature (Fransolet 1977, Smeds *et al*. 1998, Roda-Robles *et al*. 2010, 2011, Hatert *et al*. 2012b). In order to obtain a reliable and homogeneous set of data, we decided to

TABLE 4. CHEMICAL COMPOSITIONS OF SARCOPSIDE-TYPE PHOSPHATES, HYDROTHERMALLY SYNTHESIZED FROM THE $Li(Fe^{2+}_{2.5-x}Mn^{2+}_{x})(PO_4)_2$ STARTING COMPOSITIONS ($x = 0.0, 0.5, 1.0$)

Exp. no.	H.302	H.297	H.303	H.304	H.312	H.305	H.311	H.306	H.314	H.307	H.313
Number of analyses	21	18	17	17	18	16	16	15	17	28	18
X	0.0	0.0	0.0	0.5	0.5	0.5	0.5	1.0	1.0	1.0	1.0
T (°C)	400	500	600	400	500	600	700	400	500	600	700
P_2O_5 (wt.%)	38.50	39.94	40.34	40.40	39.03	40.94	39.37	42.69	40.42	40.29	38.42
FeO	60.53	60.19	58.59	48.26	50.51	47.37	40.81	32.01	41.60	30.78	31.92
MnO	0.00	0.00	0.00	11.90	9.81	11.12	19.44	25.30	18.36	29.41	28.28
Li_2O[a]	0.13	0.47	0.40	0.38	0.12	0.80	0.09	0.22	0.19	0.10	0.24
	± 0.02	± 0.05	± 0.14	± 0.04	± 0.02	0.15	± 0.03	± 0.01	± 0.10	± 0.01	± 0.05
Total	99.16	100.60	99.33	100.94	99.47	100.23	99.71	100.22	100.57	100.58	98.86
Cation numbers calculated on the basis of 8 O per formula unit											
P (*apfu*)	1.970	1.992	2.021	2.002	1.982	2.019	1.988	2.080	2.009	2.005	1.965
Fe^{2+}	3.060	2.965	2.900	2.362	2.533	2.309	2.036	1.541	2.043	1.513	1.613
Mn^{2+}	0.000	0.000	0.000	0.590	0.498	0.549	0.982	1.234	0.913	1.464	1.447
Li	0.030	0.111	0.096	0.090	0.029	0.188	0.022	0.051	0.045	0.023	0.058
Fe/(Fe + Mn)	1.000	1.000	1.000	0.800	0.836	0.808	0.675	0.555	0.691	0.508	0.527

Analysts H.-J. Bernhardt (Bochum, Germany) and P. de Parseval (Toulouse, France).
[a] The Li_2O content was determined by SIMS (Analyst L. Ottolini, Pavia, Italy), and the error represents (1σ) standard deviation.

investigate natural assemblages from several pegmatites located in Spain, Portugal, Namibia, Argentina, and Brazil. A summary of the investigated samples, as well as some basic geological data concerning the pegmatites from which they were collected, are given in Table 6. Petrographic descriptions of these samples indicate that they generally consist of sarcopside lamellae included in triphylite or in ferrisicklerite [$Li_{1-x}(Fe^{3+},Mn^{2+})PO_4$] (Fig. 4c), but sometimes thin sarcopside lamellae have been observed in massive triphylite (Fig. 4d). The presence of tiny triphylite lamellae, included in larger sarcopside lamellae, is known in the Cañada pegmatite (Fig. 4c), as well as sarcopside rims surrounding ferrisicklerite grains included in a graftonite matrix (Table 6; Roda-Robles *et al*. 2004). In the La Empleada pegmatite, Argentina, a Mn-rich assemblage is observed, with tiny exsolution lamellae of zavalíaite [$(Mn^{2+},Fe^{2+})_3(PO_4)_2$] included in lithiophilite (Hatert *et al*. 2012b).

Results of the electron-microprobe analyses, performed on these phosphate assemblages, are given in Tables 7 and 8, as well as the modal proportions (fraction of exsolution lamellae in the host phase) measured with the polarizing microscope. The Fe/(Fe + Mn) ratios of the phosphates are in the range 0.76–0.83 for the Spanish and Brazilian samples, as well as for the samples from Abbabis I, whereas these ratios decrease significantly in the samples from Tsaobismund (0.63–0.64), Portugal (0.52–0.53), and Argentina (0.43–0.48) (Tables 7 and 8). Modal proportions clearly indicate a dominance of triphylite-lithiophilite in the assemblages, with amounts between 66 and 94%, except in sample AB-2B from the Cañada pegmatite, in which the amount of triphylite is only 30% (Tables 7 and 8).

The electron-microprobe analyses of natural phosphates, as well as those of synthetic phases, have been plotted on a ternary Li–(Fe + Mg)–Mn diagram (Fig. 5), in order to compare their compositions. From this diagram, it clearly appears that the compositions of natural and synthetic phosphates are very close to each other, thus making possible the use of our experimental data for thermometric applications. Moreover, the substitution mechanism $Li^+ + Li^+ = \square + Fe^{2+}$, responsible for the miscibility between triphylite and sarcopside in the experiments, is clearly observed on the ternary diagram. It is important to underline that the low Li-content of some natural triphylites, reported on Figure 5, is due to their progressive oxidation to ferrisicklerite, not to the miscibility between triphylite and sarcopside.

Experimental Phase Relations

Results between 400 and 700 °C (NNO, P = 1 kbar)

In order to understand the temperature stability and composition of the triphylite + sarcopside assemblage, hydrothermal experiments were performed at 400, 500, 600, and 700 °C (1 kbar), starting from compositions $Li(Fe^{2+}_{2.5-x}Mn^{2+}_{x})(PO_4)_2$ ($x = 0.0$, 0.5, 1.0), which represent the ideal compositions of triphylite + sarcopside assemblages in which both

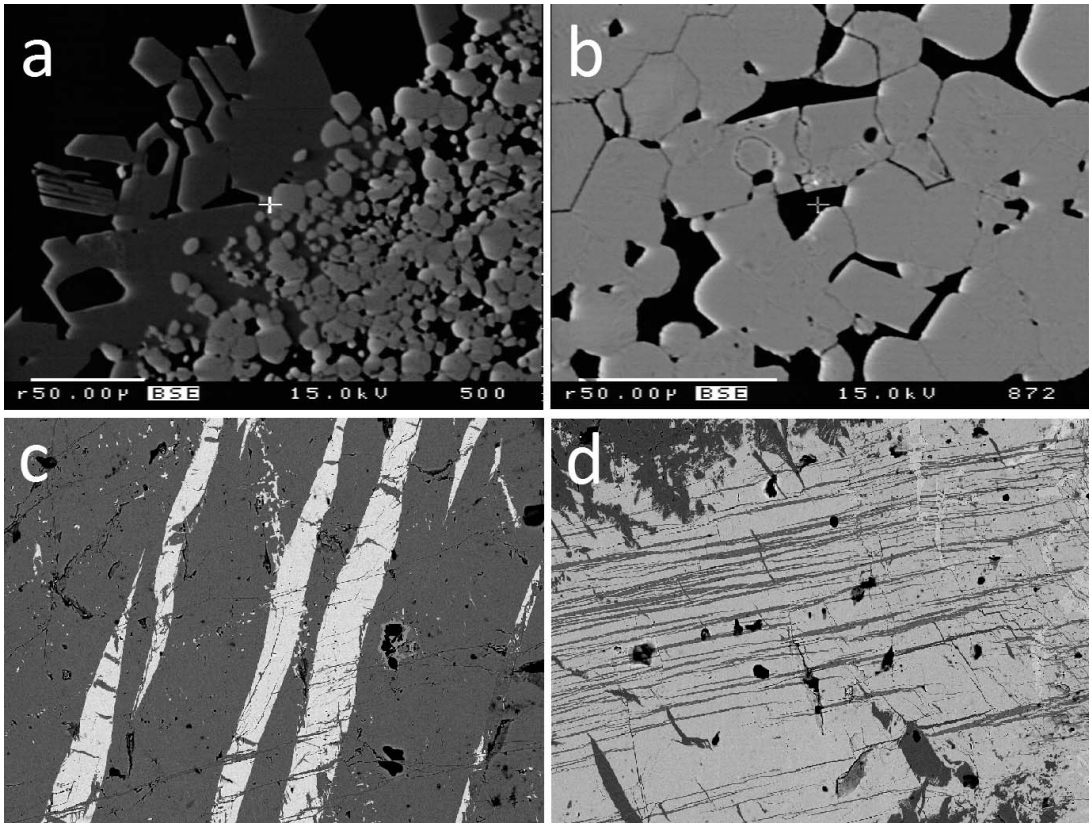

FIG. 4. (a) Assemblage of round small triphylite grains (light gray), associated with large euhedral $Fe^{2+}Fe^{3+}{}_2(PO_4)_2(OH)_2 \bullet nH_2O$ crystals (dark gray), obtained at 600 °C from the $LiFe^{2+}{}_{2.5}(PO_4)_2$ composition. Sample H.303, scanning electron microscope, backscattered electron image. (b) Euhedral crystals of $Fe^{2+}{}_2P_2O_7$ associated with round triphylite grains, obtained at 700 °C from the $LiFe^{2+}{}_{2.5}(PO_4)_2$ composition. Sample H.298, scanning electron microscope, backscattered electron image. (c) Large lamellae of sarcopside (white) included in triphylite (gray) from the Cañada pegmatite, Spain. The sarcopside lamellae themselves contain tiny triphylite lamellae. Sample SS-3-1, scanning electron microscope, backscattered electron image. (d) Thin triphylite lamellae (dark gray) included in a matrix of massive sarcopside (light gray) from the Cañada pegmatite, Spain. Sample SS-3-1, scanning electron microscope, backscattered electron image.

minerals occur in a 1:1 molar ratio. The results of these experiments (Table 1) are presented in Figure 6, which clearly shows that the triphylite + sarcopside assemblage is stable between 400 and 700 °C, sometimes associated with $Fe^{3+}{}_4(Fe^{2+},Mn^{2+})_3(PO_4)_6$, $(Fe^{2+},Mn^{2+})_2P_2O_7$, or $(Fe^{2+},Mn^{2+})Fe^{3+}{}_2(PO_4)_2(OH)_2 \bullet nH_2O$. With increasing temperature, the composition of triphylite evolves towards that of sarcopside, as shown by the decrease of their Li contents and the increase of their (Fe,Mn) contents (Table 2, Figs. 5 and 6). On the contrary, the correlation between the Li content of sarcopside and temperature does not clearly appear on Figure 6 due to a strong scatter of the data. These results indicate that a solid solution exists between triphylite and sarcopside, and that the extent of this solid solution increases with increasing temperature. As a consequence, the hypothesis of Moore (1972) is confirmed, and the lamellar textures observed in natural triphylite + sarcopside assemblages can indeed be considered as produced by exsolution processes.

At 700 °C it is still possible to distinguish sarcopside from triphylite with the scanning electron microscope (backscattered electron mode) for the Mn-bearing systems (Figs. 1b). However, the Mn-free system is characterized by similar chemical compositions for triphylite and sarcopside at this temperature, compositions which are confirmed by electron-microprobe analyses and by Rietveld refinement of the X-ray powder diffraction patterns (Figs. 1d, 4b). These observations indicate that 700 °C is close to the upper stability limit of a two-phase triphylite + sarcopside assemblage in the $LiFe^{2+}{}_{2.5}(PO_4)_2$ system.

TABLE 5. CHEMICAL COMPOSITIONS OF PHOSPHATES HYDROTHERMALLY SYNTHESIZED FROM THE $Li(Fe^{2+}_{2.5-x}Mn^{2+}_{x})(PO_4)_2$ STARTING COMPOSITIONS ($x = 0.0, 0.5, 1.0$)

	$(Fe^{2+},Mn^{2+})Fe^{3+}_2(PO_4)_2(OH)_2 \bullet nH_2O$				$Fe^{3+}_4(Fe,Mn)_3(PO_4)_6$		$(Fe^{2+},Mn^{2+})_2P_2O_7$				
Exp. no.	H.302	H.303	H.304	H.306	H.302	H.307	H.297	H.298	H.304	H.306	H.314
Number of analyses	9	10	4	3	10	3	3	5	1	6	6
P_2O_5 (wt.%)	30.88	32.09	32.27	32.98	42.87	44.64	48.86	50.35	49.85	50.60	50.51
Fe_2O_3[a]	31.79	37.50	39.70	40.40	21.11	27.87	0.00	0.00	0.00	0.00	0.00
FeO[a]	19.60	14.18	8.62	1.10	33.80	8.17	50.29	50.35	41.41	6.37	6.49
MnO	0.00	0.00	3.11	10.99	0.00	19.38	0.00	0.00	8.40	43.37	43.69
Li_2O[b]	-	0.07 ± 0.05	-	-	1.17 ± 0.02	0.99 ± 0.03	-	-	-	-	-
H_2O	17.73	16.16	16.30	14.53	-	-	-	-	-	-	-
Total	100.00	100.00	100.00	100.00	98.95	101.05	99.15	100.70	99.65	100.34	100.69
Cation numbers											
P (*apfu*)	2.000	2.000	2.000	2.000	6.000	6.000	1.991	2.007	2.006	2.010	2.004
Fe^{3+}	1.833	2.077	2.186	2.178	2.626	3.329	0.000	0.000	0.000	0.000	0.000
Fe^{2+}	1.251	0.873	0.528	0.066	4.673	1.085	2.024	1.983	1.646	0.250	0.254
Mn^{2+}	0.000	0.000	0.193	0.667	0.000	2.606	0.000	0.000	0.338	1.724	1.735
Li	-	0.022	-	-	0.776	0.629	-	-	-	-	-
H	9.042	7.934	7.960	6.942	-	-	-	-	-	-	-
Fe/(Fe + Mn)	1.000	1.000	0.934	0.771	1.000	0.629	1.000	1.000	0.830	0.127	0.128

Analysts H.-J. Bernhardt (Bochum, Germany) and P. de Parseval (Toulouse, France). Cation numbers were calculated on the basis of 2 P atoms $[(Fe^{2+},Mn^{2+})Fe^{3+}_2(PO_4)_2(OH)_2 \bullet nH_2O]$, 6 P atoms $[Fe^{3+}_4(Fe^{2+},Mn^{2+})_3(PO_4)_6]$, or 7 O atoms per formula unit $((Fe^{2+},Mn^{2+})_2P_2O_7)$.

[a] Fe_2O_3 and FeO contents were calculated to maintain charge balance.

[b] The Li_2O content was determined by SIMS (Analyst L. Ottolini, Pavia, Italy), and the error represents (1σ) standard deviation.

TABLE 6. LIST OF SELECTED SAMPLES WITH COEXISTING MEMBERS OF THE TRIPHYLITE–LITHIOPHILITE SERIES AND SARCOPSIDE, MAIN PETROGRAPHIC FEATURES, AND MAIN DATA FOR THE HOST PEGMATITES

Samples	Pegmatite	Country rock	Main minerals of the pegmatite	Phosphate associations	Phosphate textures	References
AB-XI-2R-1-1 AB-2C AB-2B AB-2-A1	Cañada (Salamanca, Spain)	Leucogranite and gabbro	Qtz, pl, kfs, ms, tur, phos	**Trp**, **sar**, **fsk**, gft, wolf, mbr	Sarcopside lamellae (tabular, lenticular, patchy, film) inside triphylite and ferrisicklerite. Often triphylite and ferrisicklerite lamellae inside the sarcopside lamellae. Sarcopside rims around granoblastic ferrisicklerite inside a matrix of granoblastic graftonite.	1
2ER	Pereña (Salamanca, Spain)	Leucogranite	Qtz, pl, kfs, ms, brl, bt, py, phos	**Fsk**, **het**, **sar**, gft, allu, stnk	Sarcopside lamellae (tabular, lenticular, patchy) inside ferrisicklerite/heterosite.	2
SA-4	NªSª de Assunçao (Aguiar, Portugal)	Two-mica granite	Qtz, pl, kfs, ms, bt, brl, phos	Trpl, **trp**, **sar**, isok, apt	Sarcopside lamellae (tabular, lenticular) inside triphylite.	3
8501-39	Tsaobismund (Karibib, Namibia)	Kfs-bearing quartzites	Qtz, pl, kfs, ms, tur, brl, col, phos	**Trp, fsk**, het, trpl, **sar**, apt, allu, beu	Sarcopside irregular grains or sarcopside lamellae (lenticular) inside triphylite/ferrisicklerite.	4
9003-14	Abbabis I (Karibib, Namibia)	Micaschists	Qtz, pl, ms, brl, col, phos	**Fsk**, **het**, **sar,** arroj Fe-wyll	Sarcopside lamellae (tabular, lenticular, patchy) inside granoblastic triphylite.	5
Boavista-1	Boavista (Galiléia, Brasil)	Schists	Qtz, pl, kfs, ms, brl, spd, phos	**Trp**, **sar**	Sarcopside lamellae (tabular, lenticular) inside triphylite.	6
EMP-1	La Empleada (San Luis, Argentina)	Micaschist	Qtz, ms, bt, pl, alm, crd, sil, phos	**Lph, zav,** red	Zavalíaite lamellae included in lithiophilite. Alteration of zavalíaite into reddingite.	7

Symbols of rock-forming minerals are taken from Kretz (1983) and Whitney & Evans (2010).
References for geological context: (1) Roda-Robles *et al.* 2004, (2) Roda-Robles *et al.* 2012a, (3) Alves 2013, (4) Fransolet *et al.* 1986, (5) Keller & Von Knorring 1989, (6) Baijot *et al.* 2012, 2014, (7) Hatert *et al.* 2012b. Symbols in bold represent the dominant phases.

TABLE 7. ELECTRON-MICROPROBE COMPOSITIONS AND MODAL PROPORTIONS OF TRIPHYLITE (OR FERRISICKLERITE)–SARCOPSIDE ASSEMBLAGES FROM SPANISH PEGMATITES

Sample	AB-XI-2R-1-1		AB-2C		AB-2B		AB-2-A1		2ER	
Pegmatite	Cañada		Cañada		Cañada		Cañada		Pereña	
Mineral	Trp	Sar	Trp	Sar	Trp	Sar	Trp	Sar	Fsk	Sar
Number of analyses	8	2	11	4	6	9	4	2	28	28
P_2O_5 (wt.%)	40.59	38.39	43.17	38.72	41.40	37.98	43.80	37.94	42.40	38.35
Fe_2O_3[a]	-	-	-	-	-	-	-	-	30.53	-
FeO[a]	37.23	48.10	35.95	45.85	39.62	48.19	35.77	47.42	11.93	46.54
MgO	1.06	0.92	1.16	0.84	1.93	1.35	1.18	0.80	0.25	0.23
ZnO	0.09	0.09	0.04	0.06	0.05	0.10	0.05	0.07	0.00	0.03
MnO	8.37	11.67	8.87	11.93	7.86	9.48	8.60	11.95	10.56	14.83
CaO	0.04	0.01	0.01	0.02	0.03	0.03	0.01	0.02	0.15	0.00
Li_2O[b]	5.78	-	7.69	-	4.89	-	8.26	-	0.00	-
Total	93.16	99.18	96.89	97.42	95.78	97.13	97.67	98.20	95.82	99.98
Cation numbers										
P (*apfu*)	1.000	1.958	1.000	1.991	1.000	1.966	1.000	1.956	1.000	1.953
Fe^{3+}	-	-	-	-	-	-	-	-	0.640	-
Fe^{2+}	0.906	2.423	0.823	2.329	0.945	2.464	0.807	2.415	0.278	2.341
Mg	0.046	0.083	0.047	0.076	0.082	0.123	0.047	0.073	0.010	0.021
Zn	0.002	0.004	0.001	0.003	0.001	0.005	0.001	0.003	0.000	0.001
Mn	0.206	0.595	0.206	0.614	0.190	0.491	0.196	0.617	0.249	0.755
Ca	0.001	0.001	0.000	0.001	0.001	0.002	0.000	0.001	0.004	0.000
Li	0.677	-	0.847	-	0.561	-	0.896	-	0.000	-
Fe/(Fe + Mn)	0.815	0.803	0.800	0.791	0.833	0.834	0.805	0.797	0.787	0.756
Modal proportions (%)	66	34	78	22	30	70	88	12	82	18
Molar proportions (%)	80	20	88	12	47	53	94	6	90	10
Calculated T (°C)	397		337		-		281		324	

Analyst P. de Parseval (Toulouse, France).
Cation numbers were calculated on the basis of 1 P *apfu* (triphylite and ferrisicklerite), or 8 O *apfu* (sarcopside).
[a] In triphylites, iron is considered as FeO, whereas in ferrisicklerite, the FeO and Fe_2O_3 contents are calculated to maintain charge balance.
[b] The Li_2O content of triphylites and ferrisicklerites was calculated to maintain charge balance.

Variations of the chemical composition with temperature

The temperature dependence of the Fe/(Fe + Mn) ratios, calculated from the electron-microprobe analyses reported in Tables 2, 4, and 5, clearly show different behavior, depending on the structural type of the synthesized phosphates. Generally, the Fe/(Fe + Mn) ratio of these phosphates is directly correlated with the bulk composition of the experimental charge, without any significant partitioning. This feature is particularly obvious for sarcopside (Table 4) and for $Fe^{3+}{}_4(Fe^{2+},Mn^{2+})_3(PO_4)_6$ (Table 5). $(Fe^{2+},Mn^{2+})Fe^{3+}{}_2(PO_4)_2(OH)_2{\bullet}nH_2O$ is significantly enriched in Fe, compared to the respective starting compositions, as shown by Fe/(Fe + Mn) values of 0.934 and 0.771 (Table 5), higher than the ideal values 0.8 ($x = 0.5$) and 0.6 ($x = 1.0$). On the contrary, $(Fe^{2+},Mn^{2+})_2P_2O_7$ shows Fe/(Fe + Mn) values as low as 0.127 (Table 5), thus indicating a strong preference of this structure type for Mn.

Figure 7 shows the variations of Li contents and Fe/(Fe + Mn) ratios of triphylites synthesized at different temperatures and coexisting with sarcopside. At 400 °C, the Li content of Mn-rich triphylite is significantly higher (0.915 Li *pfu*; Table 2) than that of Fe-rich triphylite (0.750 Li *pfu*). With increasing temperature, the Fe/(Fe + Mn) ratio of triphylites remains constant for $x = 0$ and 0.5; however, this ratio increases significantly at 600 and 700 °C for triphylites obtained from the Mn-rich starting composition $Li(Fe^{2+}{}_{1.5}Mn^{2+})(PO_4)_2$ ($x = 1$) (Fig. 7). This feature can be explained by the preference of the triphylite structure for Fe at high temperatures, and for Mn at low temperatures, as

TABLE 8. ELECTRON-MICROPROBE COMPOSITIONS AND MODAL PROPORTIONS OF TRIPHYLITE (OR FERRISICKLERITE)–SARCOPSIDE ASSEMBLAGES FROM PORTUGUESE, NAMIBIAN, BRAZILIAN, AND ARGENTINEAN PEGMATITES

Sample	SA-4		8501-39		9003-14		Boavista-1		EMP-1	
Pegmatite	N[a] S[a] de Assunçao		Tsaobismund		Abbabis I		Boavista		La Empleada	
Mineral	Trp	Sar	Trp	Sar	Fck	Sar	Trp	Sar	Lph	Zav
Number of analyses	28	28	11	8	8	13	28	27	14	27
P_2O_5 (wt.%)	44.75	42.55	43.48	38.21	48.29	41.31	45.63	39.41	48.39	41.38
Fe_2O_3[a]	-	-	-	-	34.30	-	-	-	-	-
FeO[a]	23.85	26.32	28.32	38.38	-	44.63	33.51	45.59	14.25	24.94
MgO	0.02	0.01	0.98	0.70	6.43	4.64	2.56	1.78	8.82	6.09
MnO	21.67	23.04	16.46	21.01	5.87	9.01	8.61	12.09	18.78	27.08
CaO	0.03	0.03	0.02	0.01	0.19	0.04	0.02	0.02	0.01	-
Li_2O[b]	9.18	-	8.01	-	3.90	-	9.34	-	10.19	-
Total	99.50	91.95	97.27	98.31	98.98	99.63	99.67	98.89	100.44	99.49
Cation numbers										
P (*apfu*)	1.000	2.189	1.000	1.963	1.000	2.008	1.000	1.985	1.000	1.995
Fe^{3+}	-	-	-	-	0.631	-	-	-	-	-
Fe^{2+}	0.526	1.338	0.643	1.948	-	2.143	0.725	2.269	0.291	1.188
Mg	0.001	0.001	0.040	0.063	0.234	0.397	0.099	0.158	0.321	0.517
Mn	0.484	1.186	0.379	1.080	0.122	0.438	0.189	0.609	0.388	1.307
Ca	0.001	0.002	0.001	0.001	0.005	0.002	0.001	0.001	0.001	-
Li	0.975	-	0.875	-	0.384	-	0.973	-	1.000	-
Fe/(Fe + Mn)	0.521	0.530	0.629	0.643	0.838	0.830	0.793	0.788	0.429	0.476
Modal proportions (%)	90	10	85	15	85	15	93	7	94	6
Molar proportions (%)	95	5	92	8	92	8	96	4	97	3
Calculated T (°C)	322		330		301		276		319	

Analyst P. de Parseval (Toulouse, France).
Cation numbers were calculated on the basis of 1 P *apfu* (lithiophilite, triphylite, and ferrisicklerite), or 8 O *apfu* (sarcopside and zavalíaite).
[a] In triphylites and lithiophilites, iron is considered as FeO, whereas in ferrisicklerite, the FeO and Fe_2O_3 contents are calculated to maintain charge balance.
[b] The Li_2O content of triphylites, lithiophilites, and ferrisicklerites was calculated to maintain charge balance.

previously observed for alluaudite-type phosphates (Hatert *et al*. 2006).

Development of a Triphylite–Sarcopside Geothermometer

According to Figure 6, a broad miscibility gap exists between the non-isostructural phases triphylite and sarcopside in the $Li(Fe^{2+}_{2.5-x}Mn^{2+}_{x})(PO_4)_2$ (x = 0.0, 0.5, 1.0) system. As this gap is temperature-dependent, it can be generally used as a geothermometer where triphylite and sarcopside coexist. In such a case, measurement of the proportions of both phosphates in a natural sample, *e.g*., proportions of triphylite matrix and of the sarcopside exsolution lamellae, allows us to determine the composition of the primary, high-temperature phase in the $Li_2(Fe^{2+},Mn^{2+})_2(PO_4)_2$–$(Fe^{2+},Mn^{2+})_3(PO_4)_2$ binary system and place a minimum constraint on the crystallization temperature.

In the triphylite-type region the solvus was found to be compositionally dependent and can therefore be used as a geothermometer in order to determine a minimum temperature of sarcopside exsolution from a triphylite host. This feature clearly appears on Figure 8, where the compositions of triphylites and sarcopsides synthesized from the three different starting compositions are plotted together. We first attempted to establish a thermodynamic model to fit the experimental data; however, this solid solution model was very complex and did not facilitate extraction of any thermodynamic parameters. We decided then, for each starting composition, to simply fit the experimental data with linear regressions; the equations and correlation coefficients for these three fits are shown in Figure 8. The three linear fits are in good agreement with the experimental data, and show a displacement

when the Fe/(Fe + Mn) ratio of the starting composition changes. For the Mn-free system, the linear regression line lies in Li-poor compositions, while for Mn-rich systems the line evolves towards Li-rich compositions.

Even if the regression lines show significant displacements depending on the starting composition, they have similar slopes and are parallel to each other on the diagram (Fig. 8). For this reason, it is possible to establish a global equation which allows us to determine the exsolution temperature from the Li content and Fe/(Fe + Mn) ratio of the starting composition. This equation can be expressed as: T (°C) = (–142 × XFe) – (773 × Li *pfu*) + 1131, where XFe = Fe/(Fe + Mn). Temperatures, calculated with this equation from the compositions of synthetic triphylites, are in good agreement with the synthesis conditions; the average uncertainty is around ±15 °C. For rare-element pegmatites (Černý & Ercit 2005) the relevant pressures are generally in the range $0.2 \geq P \geq 0.4$ GPa, which is substantially lower than those for metamorphic rocks. Therefore, we can assume that the pressure-dependent contribution to the above equation can be neglected. However, this equation does not take into account the presence of Mg in the system, which would significantly modify the exsolution temperatures, as discussed below.

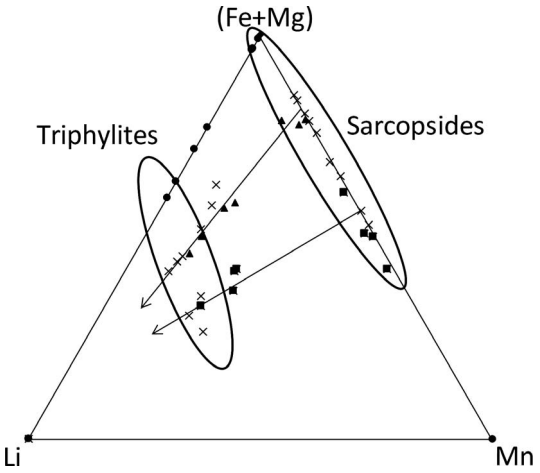

FIG. 5. Ternary Li–(Fe + Mg)–Mn diagram showing the compositions of synthetic and natural triphylites and sarcopsides investigated in this paper. The arrows indicate the substitution mechanism $Li^{+} + Li^{+} = Fe^{2+} + \square$. Crosses = natural samples, circles = $LiFe^{2+}{}_{2.5}(PO_4)_2$ system, triangles = $Li(Fe^{2+}{}_2Mn^{2+}{}_{0.5})(PO_4)_2$ system, squares = $Li(Fe^{2+}{}_{1.5}Mn^{2+})(PO_4)_2$ system.

DISCUSSION

Structural relationships between triphylite and sarcopside, and stability of $LiFePO_4$

The experimental results reported in this paper indicate that partial miscibility exists between triphylite and sarcopside, and that the extent of the solid solution between these two minerals increases with increasing temperature. The miscibility between triphylite and sarcopside is due to the structural similarities between these two phosphates: the two structures are not isotypic but are topologically related (Fig. 9).

Triphylite crystallizes in the orthorhombic space group *Pbnm* and sarcopside in the monoclinic space group $P2_1/c$. In both structures the PO_4 tetrahedra and the M octahedra are arranged in the same way. The M2 position is completely occupied by Fe, and both phases mainly differ in the occupancy of the M1 position. In triphylite the M1 site is occupied by Li, while in sarcopside, it is occupied by Fe and alternates with a structurally unoccupied position V (Fig. 9). Both positions M1 and V of the sarcopside structure are the equivalent of the M1 position in the triphylite structure.

A simple model for the formation of solid solutions of sarcopside type (Fig. 9) includes replacement of Fe at the M1 position of the sarcopside structure by Li, and a partial occupancy of the vacant position V by an equivalent amount of Li. On the other hand, a solid solution with the triphylite structure includes a disordered substitution of Li at the M1 position of triphylite by Fe and vacancies.

Electron-microprobe and SIMS analyses of the synthesized phosphates indicate that Fe-rich triphylites show very low Li-contents at 400 °C compared to Mn-rich triphylites (Figs. 7 and 8). This observation raises the question of $LiFe^{2+}PO_4$ stability. Indeed, in the literature, $LiFe^{2+}PO_4$ is frequently synthesized for its application in Li-ion batteries, but its Li content is generally considered to be stoichiometric, without any confirmation by chemical analysis. The SIMS results given in this paper (Fig. 7), as well as the low Li contents of Fe-rich triphylites synthesized by Hatert *et al*. (2011), seem to confirm that stoichiometric $LiFe^{2+}PO_4$ is not a stable phase at low temperature. This feature certainly explains the higher Li contents of natural lithiophilites (1.07–1.15 Li *pfu*) compared to the Li contents of natural triphylites (0.99–1.04 Li *pfu*) measured by Hatert (2012).

The Li content of triphylite-type phosphates is governed by crystal-chemical constraints. A structural study of the lithiophilite-sicklerite solid solution demonstrated the strong inverse correlation between M1–O and M2–O distances in these phosphates (Hatert *et al*. 2012a). In triphylite, Fe^{2+} occurs at the

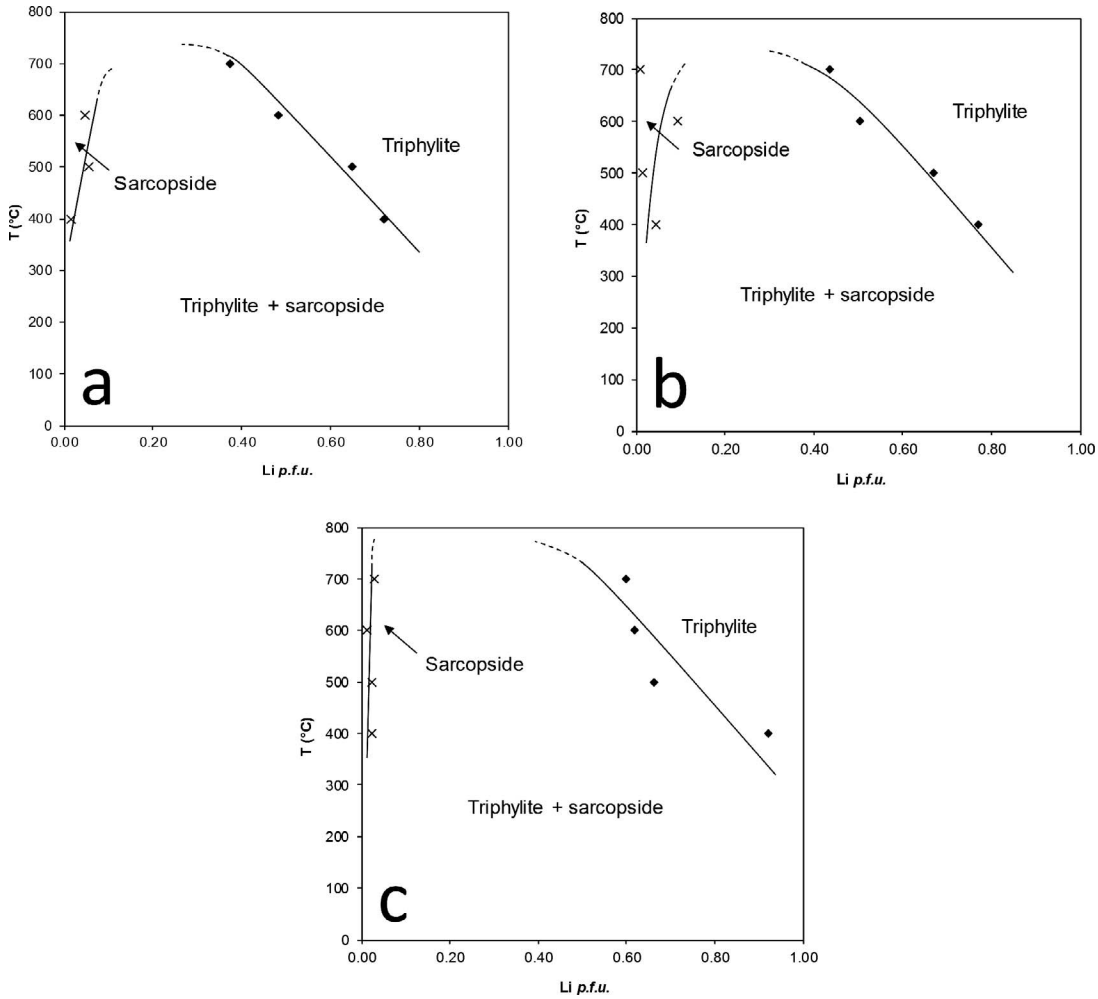

FIG. 6. Diagrams showing the phase relations in the $Li(Fe^{2+}_{2.5-x}Mn^{2+}_{x})(PO_4)_2$ ($x = 0.0, 0.5, 1.0$) system between 400 and 700 °C (P = 1 kbar). Starting compositions are: (a) $LiFe^{2+}_{2.5}(PO_4)_2$; (b) $Li(Fe^{2+}_{2}Mn^{2+}_{0.5})(PO_4)_2$; (c) $Li(Fe^{2+}_{1.5}Mn^{2+})(PO_4)_2$.

M2 site, and its small ionic radius (effective ionic radius, *eir*, 0.780 Å; Shannon 1976) implies short M2–O bond lengths compared to those of lithiophilite in which M2 is occupied by Mn^{2+} (*eir* 0.830 Å). The short M2–O bond lengths in triphylite consequently induce an increase of the M1–O bond lengths; the M1 site then becomes too large to be completely occupied by Li owing to bond valence requirements. This mechanism obviously explains the low Li contents of synthetic triphylites.

Geothermometric applications

In the present study the triphylite + sarcopside assemblage was obtained experimentally for the first time; this experimental evidence corroborates the primary origin of the triphylite + sarcopside assemblage in granitic pegmatites. Moreover, the phase diagrams in Figure 6 indicate an extended miscibility between triphylite and sarcopside at 700 °C. The shape of the solvus, particularly the broadening with decreasing temperature, facilitates exsolution upon cooling, thus confirming the formation process of lamellar triphylite–sarcopside intergrowths in pegmatites.

The triphylite + sarcopside geothermometer presented in this paper can be applied to natural assemblages by measuring the modal proportions of triphylite and sarcopside in the exsolution textures. These proportions were measured on the samples reported in Tables 7 and 8; the values were then

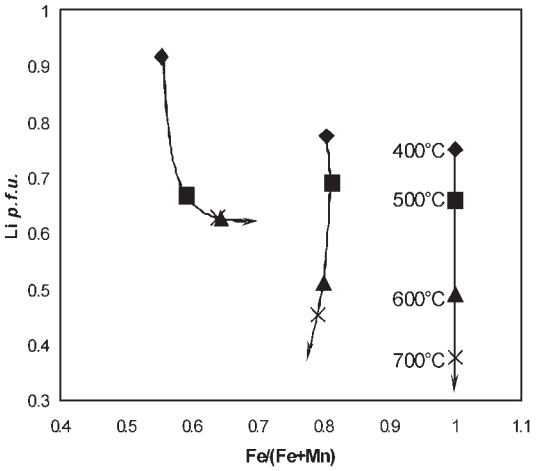

FIG. 7. Diagram showing the temperature dependence of the average Fe/(Fe + Mn) ratios and Li contents for triphylites synthesized in the $Li(Fe^{2+}_{2.5-x}Mn^{2+}_{x})(PO_4)_2$ ($x = 0.0$, 0.5, 1.0) system. Diamonds = 400 °C, squares = 500 °C, triangles = 600 °C, and crosses = 700 °C. The arrows indicate temperature increase.

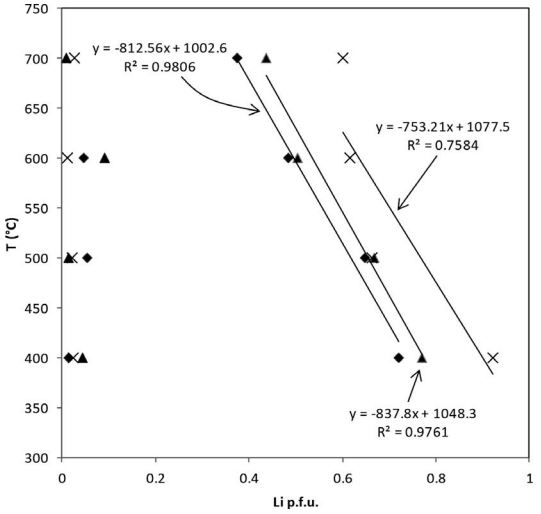

FIG. 8. Phase diagram showing the fits of the experimental data for synthetic triphylites obtained from the three starting compositions. Diamonds = $LiFe^{2+}_{2.5}(PO_4)_2$ system, triangles = $Li(Fe^{2+}_{2}Mn^{2+}_{0.5})(PO_4)_2$ system, crosses = $Li(Fe^{2+}_{1.5}Mn^{2+})(PO_4)_2$ system.

multiplied by the densities and divided by the molar weights of the phosphates to obtain molar proportions. These proportions were introduced in the equation given above to calculate the exsolution temperatures reported in the last line of Tables 7 and 8. These temperatures range from 276 to 397 °C and are in very good agreement with the experimental data obtained by Hatert *et al*. (2006) for the $Na_2(Mn_{2-2x}Fe_{1+2x})(PO_4)_3$ system, with the temperatures obtained by Hatert *et al*. (2011) from the Na-in-triphylite geothermometer, and with the temperatures generally accepted for the formation of primary minerals in rare-element granitic pegmatites (London 2008, London *et al*. 2012).

The samples from the Cañada pegmatite, Spain, show exsolution temperatures between 281 and 397 °C; the temperature for sample AB-2B was not calculated because the geothermometer cannot be applied to assemblages in which sarcopside dominates. According to Roda-Robles *et al*. (2004), these samples were collected in the Inner Zone of the pegmatite; the temperature of the Outer Zone was calculated by using several garnet-biotite geothermometers, and corresponds to 537–558 °C (E. Roda-Robles, *pers. commun*.). The lower temperatures obtained for the Inner Zone, compared to those of the Outer Zone, confirm the temperature trends generally accepted for pegmatite differentiation and crystallization processes.

The relatively large temperature range calculated with the triphylite–sarcopside geothermometer for the Cañada assemblages could be explained by temperature zoning within phosphate nodules. Such a zoning was observed in a large phosphate nodule (*ca*. 70 cm diameter) from the Jocão pegmatite, Minas Gerais, Brazil, in which beusite exsolution lamellae occur in triphylite (Baijot *et al*. 2014). The amount of triphylite is significantly higher on the border of the nodule (29 vol.% triphylite), thus indicating a lower exsolution temperature, compared to that of the core assemblages in which triphylite is less abundant (24 vol.% triphylite). A similar process is certainly responsible for the wide exsolution temperature range of the Cañada assemblages, since these phosphates also occur in large nodules attaining 1 m diameter, in which a temperature zoning may be expected. The higher calculated temperature, 397 °C, is closer to the crystallization temperature of host silicate assemblages from the Inner Zone, and the lower temperature of 281 °C was certainly achieved during the cooling of the border of the nodule.

Sample EMP-1 from the La Empleada pegmatite, Argentina, is particularly rich in Mn; the phosphates involved in the exsolution textures are the Mn-rich endmembers zavalíaite, $(Mn^{2+},Fe^{2+})_3(PO_4)_2$ (Hatert *et al*. 2012b), and lithiophilite, $Li(Mn^{2+},Fe^{2+})PO_4$. According to the general Mn-enrichment process, which affects mineral solid solutions during the differentiation of pegmatites (Baldwin & Von Knorring 1983, Černý *et al*. 1985), we would expect a very low exsolution temperature for these assemblages; howev-

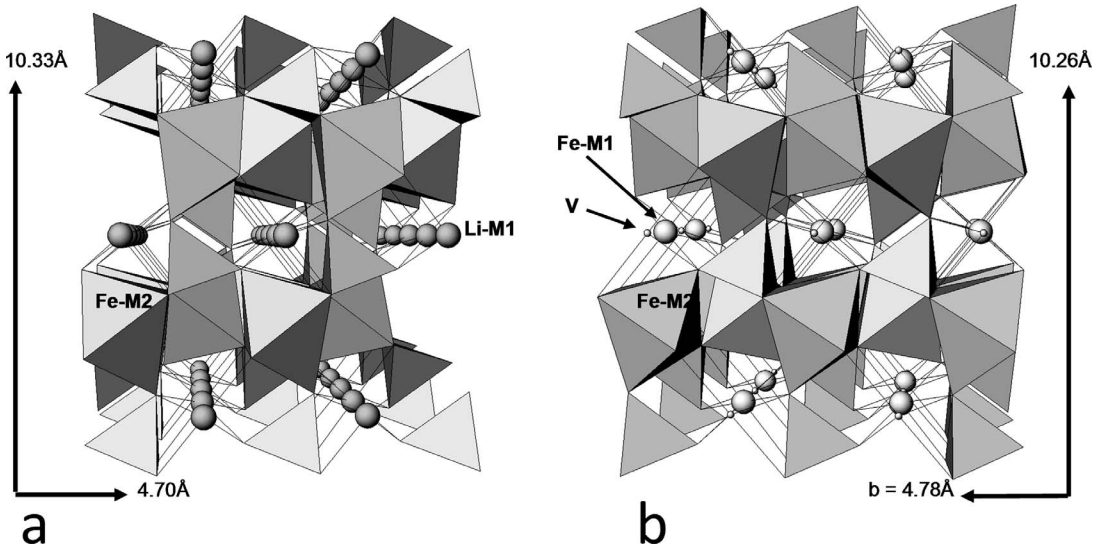

FIG. 9. Comparison between the triphylite (a; *Pbmn*) and sarcopside (b; $P2_1/c$) structures.

er, a temperature of 319 °C was obtained for sample EMP-1 (Table 8), comparable to the temperatures obtained for other assemblages. This relatively high exsolution temperature indicates that phosphate assemblages from the La Empleada pegmatite are weakly differentiated; this weak differentiation is confirmed by the particularly high Mg contents of the phosphates (Table 8). These high Mn contents can be explained by the presence of large schorl and garnet crystals among host silicates. The crystallization of Fe-rich silicates reduced the available Fe, thus producing phosphates particularly enriched in Mn. A similar feature has recently been observed in the Cema pegmatite, close to La Empleada, where Mn-rich phosphate assemblages also occur (Roda-Robles *et al*. 2012b).

Generally, it is accepted that Mn-rich members of solid solutions crystallize at low temperatures in pegmatites (Baldwin & Von Knorring 1983, Černý *et al*. 1985, Hatert *et al*. 2006). However, despite their high Mn contents, phosphates from La Empleada indicate a rather high exsolution temperature, which seems to be contradictory with the generally accepted geochemical trends. A careful examination of the experimental phase diagrams obtained in this study (Figs. 6, 8) indicates that the exsolution temperatures are higher for Mn-rich systems, compared to the Mn-free system. For this reason, the Mn-free system shows a nearly complete solid solution at 700 °C, while the Mn-bearing systems contain both triphylite and sarcopside at this temperature. More extensive miscibility between phosphates crystallizing in the Fe-rich system is controlled by crystal-chemical constraints. In the triphylite–sarcopside solid solution, the substitution of Li (*eir* 0.76 Å) is more feasible by Fe^{2+} (*eir* 0.780 Å) than by the larger Mn^{2+} (*eir* 0.830 Å). As a consequence, Fe-rich triphylite–sarcopside assemblages show low exsolution temperatures. It is important to note that these temperatures do not represent the crystallization temperatures of the phosphate nodules, but an exsolution temperature which corresponds to the closing temperature of the triphylite–sarcopside element exchange. It is therefore not surprising that the exsolution textures indicate temperatures which may be significantly lower than those expected from the pegmatite geochemical trends.

Finally, a last comment concerns the Mg contents of the phosphates, which are particularly high in samples 9003-14, Boavista-1, and EMP-1 (Table 8). The influence of Mg has not been taken into account in the experiments presented in this paper, and the exsolution temperatures obtained for these assemblages have to be used with caution. According to the crystal-chemical considerations described above, the small ionic radius of Mg^{2+} (*eir* 0.720 Å) would favor its substitution relative to Li in the triphylite–sarcopside solid solutions, thus increasing the miscibility between the Mg-rich endmembers. The presence of significant amounts of Mg in the phosphates would consequently result in a significant lowering of the exsolution temperature.

Acknowledgments

Many thanks are due to Lee Groat and Pietro Vignola for editorial help, to Fabrice Brunet for his constructive comments, and to H.-J. Bernhardt (Bochum) and Philippe de Parseval (Toulouse) who obtained the electron-microprobe analyses. FH thanks the F.N.R.S. (Belgium) for the position of "Chercheur qualifié", for grants 1.5.113.05.F and 1.5.098.06.F, and for FRIA grant 1.E148.13. ERR thanks the Spanish Ministerio de Economia y Competitividad (Project CGL 2012-31356) for financial support.

References

Baijot, M., Hatert, F., & Philippo, S. (2012) Mineralogy and geochemistry of phosphates and silicates in the Sapucaia pegmatite, Minas Gerais, Brazil: Genetic implications. *Canadian Mineralogist* **50**, 1531–1554.

Baijot, M., Hatert, F., Dal Bo, F., & Philippo, S. (2014) Mineralogy and petrography of phosphate mineral associations from the Jocão pegmatite, Minas Gerais, Brazil. *Canadian Mineralogist* **52**, 373–397.

Baldwin, J.R. & Von Knorring, O. (1983) Compositional range of Mn-garnet in zoned granitic pegmatites. *Canadian Mineralogist* **21**, 683–688.

Belfguira, N., Walha, S., Ben Salah, A., Hatert, F., Fransolet, A.-M., & Kabadou, A. (2010) Hydrothermal synthesis and structure of $Fe_{6.36}Mn_{0.64}(PO_3(OH))_4(PO_4)_2$. *Journal of Chemical Crystallography* **40**, 1125–1128.

Brunet, F., Chopin, C., & Seifert, F. (1998) Phase relations in the $MgO–P_2O_5–H_2O$ system and the stability of phosphoellenbergerite: Petrological implications. *Contributions to Mineralogy and Petrology* **131**, 54–70.

Burnham, C.W. (1991) *LCLSQ version 8.4, least-squares refinement of crystallographic lattice parameters*. Department of Earth Planetary Sciences, Harvard University, Cambridge, Massachusetts, 24 pp.

Černý, P. & Ercit, T.S. (2005) The classification of granitic pegmatites revisited. *Canadian Mineralogist* **40**, 2005–2026.

Černý, P., Meintzer, R.E., & Anderson, A.J. (1985) Extreme fractionation in rare-element granitic pegmatites: Selected examples of data and mechanisms. *Canadian Mineralogist* **23**, 381–421.

Dal Bo, F. & Hatert, F. (2012) $Fe(II)_{2.67}Fe(III)_4(PO_4)_{5.35}(HPO_4)_{0.65}$ and $Fe(II)_{2.23}Fe(III)_4(PO_4)_{4.45}(HPO_4)_{1.55}$, two new mixed-valence iron phosphates. *Acta Crystallographica* **C68**, i83–i85.

Fransolet, A.-M. (1975) *Etude minéralogique et pétrologique des phosphates de pegmatites granitiques*. Ph.D. Thesis, University of Liège, Liège, Belgium, 333 pp.

Fransolet, A.-M. (1977) Intercroissances et inclusions dans les associations graftonite-sarcopside-triphylite. *Bulletin de la Société française de Minéralogie et de Cristallographie* **100**, 198–207.

Fransolet, A.-M., Keller, P., & Fontan, F. (1986) The phosphate mineral associations of the Tsaobismund pegmatite, Namibia. *Contributions to Mineralogy and Petrology* **92**, 502–517.

Hatert, F. (2012) Iron-manganese phosphates with the olivine- and alluaudite-type structures: crystal chemistry and applications. *In* Minerals as Advanced Materials II (S. Krivovichev, ed.). Springer-Verlag, Berlin-Heidelberg, Germany (279–292).

Hatert, F., Fransolet, A.-M., & Maresch, W.V. (2006) The stability of primary alluaudites in granitic pegmatites: an experimental investigation of the $Na_2(Mn_{2-2x}Fe_{1+2x})(PO_4)_3$ system. *Contributions to Mineralogy and Petrology* **152**, 399–419.

Hatert, F., Ottolini, L., & Schmid-Beurmann, P. (2011) Experimental investigation of the alluaudite + triphylite assemblage, and development of the Na-in-triphylite geothermometer: applications to natural pegmatite phosphates. *Contributions to Mineralogy and Petrology* **161**, 531–546.

Hatert, F., Ottolini, L., Wouters, J., & Fontan, F. (2012a) A structural study of the lithiophilite–sicklerite series. *Canadian Mineralogist* **50**, 843–854.

Hatert, F., Roda-Robles, E., de Parseval, P., & Wouters, J. (2012b) Zavalíaite, $(Mn^{2+},Fe^{2+},Mg)_3(PO_4)_2$, a new member of the sarcopside group from the La Empleada pegmatite, San Luis Province, Argentina. *Canadian Mineralogist* **50**, 1445–1452.

Hatert, F., Baijot, M., & Dal Bo, F. (2014) The stability of Fe-rich alluaudites in granitic pegmatites: An experimental investigation of the $Na–Fe^{2+}–Fe^{3+}$ $(+PO_4)$ system. *Canadian Mineralogist* **52**, 351–371.

Keller, P. & Von Knorring, O. (1989) Pegmatites at the Okatjimukuju farm, Karibib, Namibia. Part I: Phosphate mineral associations of the Clementine II pegmatite. *European Journal of Mineralogy* **1**, 567–593.

Kretz, R. (1983) Symbols for rock-forming minerals. *American Mineralogist* **68**, 277–279.

London, D. (2008) Pegmatites. *Canadian Mineralogist Special Publication* **10**, 347 pp.

London, D., Wolf, M.B., Morgan, G.B., & Gallego Garrido, M. (1999) Experimental silicate-phosphate equilibria in peraluminous granitic magmas, with a case study of the Albuquerque batholith at Tres Arroyos, Badajoz, Spain. *Journal of Petrology* **40**, 215–240.

London, D., Morgan, G.B., & Wolf, M.B. (2001) Amblygonite–montebrasite solid solutions as monitors of fluorine in evolved granitic and pegmatitic melts. *American Mineralogist* **86**, 225–233.

London, D., Morgan, G.B., Paul, K.A., & Guttery, B.M. (2012) Internal evolution of miarolitic granitic pegmatites at the little three mine, Ramona, California, USA. *Canadian Mineralogist* **50**, 1025–1054.

Moore, P.B. (1965) The crystal structure of laueite, $Mn^{2+}Fe^{3+}{}_2(OH)_2(PO_4)_2(H_2O)_6{\bullet}2H_2O$. *American Mineralogist* **60**, 1884–1892.

Moore, P.B. (1972) Sarcopside: its atomic arrangement. *American Mineralogist* **57**, 24–35.

O'Neill, H.S.C. & Pownceby, M.I. (1993) Thermodynamic data from redox reactions at high temperatures. I. An experimental and theoretical assessment of the electrochemical method using stabilized zirconia electrolytes, with revised values for the Fe–"FeO", Co–CoO, Ni–NiO, and Cu–Cu_2O oxygen buffers, and new data for the W–WO_2 buffer. *Contributions to Mineralogy and Petrology* **114**, 296–314.

Ottolini, L., Bottazzi, P., & Vannucci, R. (1993) Quantification of lithium, beryllium and boron in silicates by secondary ion mass spectrometry using conventional energy filtering. *Analytic Chemistry* **65**, 1960–1968.

Rietveld, H.M. (1967) Line profiles of neutron powder-diffraction peaks for structure refinements. *Acta Crystallographica* **22**, 151–152.

Rietveld, H.M. (1969) A profile refinement method for nuclear and magnetic structures. *Journal of Applied Crystallography* **2**, 65–71.

Roda-Robles, E., Pesquera, A., Fontan, F., & Keller, P. (2004) Phosphate mineral associations in the Cañada pegmatite (Salamanca, Spain): Paragenetic relationships, chemical compositions, and implications for pegmatite evolution. *American Mineralogist* **89**, 110–125.

Roda-Robles, E., Nizamoff, J.W., Simmons, W.B., Falster, A.U., & Hatert, F. (2010) Graftonite-triphylite-sarcopside intergrowths from the Palermo No. 1 pegmatite (New Hampshire, USA): textures and chemistry. *Acta Mineralogica-Petrographica*, *Abstract series* **6**, 618.

Roda-Robles, E., Galliski, M., Nizamoff, J.W., Simmons, W., Keller, P., Falster, A., & Hatert, F. (2011) Cation partitioning between minerals of the triphylite ± graftonite ± sarcopside association in granitic pegmatites. Abstract book from the 5th International symposium on granitic pegmatites, PEG 2011, 161–164.

Roda-Robles, E., Pesquera, A., Gil-Crespo, P.P., & Torres-Ruiz, J. (2012a) The Puentemocha beryl-phosphate granitic pegmatite, Salamanca, Spain: Internal structure, petrography and mineralogy. *Canadian Mineralogist* **50**, 1573–1587.

Roda-Robles, E., Galliski, M., Roquet, M.B., Hatert, F., & de Parseval, P. (2012b) Phosphate nodules containing two distinct assemblages in the Cema granitic pegmatite, San Luis Province, Argentina: Paragenesis, composition and significance. *Canadian Mineralogist* **50**, 913–931.

Rondeux, M. (2011) *Etude expérimentale de la cristallochimie et de la stabilité des phosphates à structure fillowite*. Ph.D. thesis, University of Liège, Liège, Belgium, 238 pp.

Shannon, R.D. (1976) Revised effective ionic radii and systematic studies of interatomic distances in halides and chalcogenides. *Acta Crystallographica* **A32**, 751–767

Smeds, S.T., Uher, P., Černý, P., Wise, M.A., Gustafsson, L., & Penner, P. (1998) Graftonite-beusite in Sweden: Primary phases, products of exsolution, and distribution in zones populations of granitic pegmatites. *Canadian Mineralogist* **36**, 377–394.

Stefanidis, T. & Nord, A.G. (1982) The crystal structure of iron(II) diphosphate, $Fe_2P_2O_7$. *Zeitschrift für Kristallographie* **159**, 255–264.

Stefanidis, T. & Nord, A.G. (1984) Structural studies of thortveitite-like dimanganese diphosphate, $Mn_2P_2O_7$. *Acta Crystallographica* **C40**, 1995–1999.

Tuttle, O.F. (1949) Two pressure vessels for silicate-water studies. *Geological Society of America Bulletin* **60**, 1727–1729.

Whitney, L.D. & Evans, B.W. (2010) Abbreviations for names of rock-forming minerals. *American Mineralogist* **95**, 185–187.

Young, R.A., Larson, A.C., & Paiva-Santos, C.O. (1998) *User's guide to program DBWS-9807 for Rietveld analysis of X-ray and neutron powder diffraction patterns*. School of Physics, Georgia Institute of Technology, Atlanta, Georgia, United States, 56 pp.

Received February 1, 2016. Revised manuscript accepted May 27, 2016.